Progress In Electromagnetics Research M, Vol. 139, 104–114, 2026

PIER M

(Received 8 June 2026, Accepted 23 July 2026, Scheduled 5 September 2026)

Quadruple Concentric Split Ring Resonators-Based Dual Broadband Metamaterial Absorber for X- and Ku-Band Applications

Supriya, Alkesh Agrawal*, Bhagwant Singh, and Vijay Tiwari

Shri Ramswaroop Memorial University, Barabanki 225003, U.P., India

ABSTRACT: This manuscript presents a simple, novel design of a dual broadband absorber with merged double bands and double-split concentric ring resonators in each quadrant-based metamaterial absorber (DBBMDBMMA). The proposed structure exhibits two experimentally validated absorptance broadbands; one extending from 7.73 GHz–9.54 GHz and the other extending from 10.65 GHz–13.27 GHz. The two broadbands cover X-band and Ku-band, respectively. The DBBMDBMMA is fabricated on a double-sided FR4 copper plate with electrical dimensions of $0.5\lambda_o \times 0.5\lambda_o \times 0.05\lambda_o$ (λ_o at 8.5 GHz). The unit cell of the metamaterial absorber consists of concentric double split-ring resonators in each quadrant, with splits oriented vertically opposite and separated by a 90° inclination difference. The novelty lies in the response and design of the proposed structure that exhibits dual broadbands extending in two microwave bands without using parasitic elements, a multilayered structure, or an extended substrate width. The response of the DBBMDBMMA structure is stable with variation in incidence and polarization angle. The metamaterial behaviour is studied in terms of effective values of normalized matched impedance, permeability, and permittivity. The proposed DBBMDBMMA exhibits reflectance of -21.62 dB at 8.59 GHz, -26.18 dB at 8.88 GHz, -15.11 dB at 11.24 GHz, and -18.63 dB at 12.86 GHz. The first absorptance peak is contributed by outer split-ring resonators in quadrants II and IV; the second absorptance peak is contributed by outer split-ring resonators in quadrants I and III; the third absorptance peak is contributed by inner split-ring resonators in quadrants II and IV; and the fourth absorptance peak is contributed by inner split-ring resonators in quadrants I and III. The proposed DBBMDBMMA structure exhibits polarization and wide incident angle insensitive response that finds applications in stealth technology and RCS reduction.

1. INTRODUCTION

"Metamaterial" is an artificially engineered substance with an unusual structure and exceptional properties of negative μ, negative ε, and negative η [1]. Metamaterial absorbers (MMAs) have gained popularity over the past few years because of their special qualities, which include ultrathin dimensions, compact design, affordability, and easily adjustable characteristics [2]. Metamaterials have a wide range of possible uses due to their unique electromagnetic (EM) properties [3]. This has resulted in the development of numerous beneficial applications, such as "sensing" [4], "energy harvesting" [5], "filters" [6], "perfect absorbers" [7], "radar and satellite communications" [8], "electromagnetic wave stealth" [9], "optical switches and filters" [10], and "multi-band electromagnetic wave concealment" [11]. Since high-absorption MMA with a single band is unsuitable for many applications, it is imperative to investigate wide-band or high-performance MMAs with multiple bands in compact dimensions [12, 13]. However, in MMAs, the perfect absorption phenomenon is sensitive to structural and material variations, and is readily disrupted; therefore, it is challenging to create MMAs with combined multi-bands and improved absorptance. Research is thus being driven by advancements in merged multi-band MMA design. Since Landy et al. originally presented a split-ring resonator (SRR)-based perfect MMA in 2008 [14], researchers have contributed a lot in the field of MMAs with gradual advancement in design, performance, and stable response. The broadband and multi-band (also referred to as "dual-band", "triple-band", and "quad-band") response is generated by researchers using "parasitic elements" [15], building a substrate with many layers [16], or widening the substrate [17]. However, in this manuscript, a novel MMA design is presented with experimental validation without using "parasitic elements", "multi-layered structure", or "widened substrate", which contributes to a pair of broadbands that are generated from merged dual bands in X- and Ku-bands.

Four-square SRRs with an inner star form make up the absorber proposed in [18]. Four different resonances at 4.685 GHz, 6.434 GHz, 8.0869 GHz, and 10.974 GHz are intended to produce narrow-band absorptance of 86.97%, 99.74%, 99.95%, and 98.43%, respectively, for sensor application. The absorber has overall dimensions of 10 mm $\times$ 10 mm $\times$ 1 mm. For Ku- and K-band applications, a quad-band polarization-insensitive metamaterial absorber (MMA) is proposed in [19]. In order to produce four comparable resonances at 12.62 GHz, 14.12 GHz, 17.53 GHz, and 19.91 GHz with 97%, 99.51%, 99%, and 99.5% absorption, respectively, the proposed patch has an inner Jerusalem cross, four microstrip

* Corresponding author: Alkesh Agrawal (alkesh.agrawal26@gmail.com).

doi:10.2528/PIERM26060806

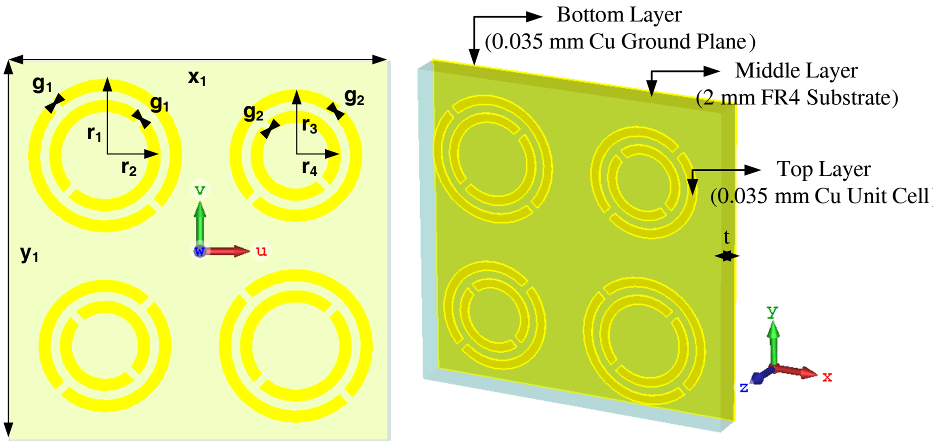

FIGURE 1. Dimensional structure of DBBMDBMMA unit cell.

lines, and two square split-ring resonators (SSRRs). The rotational symmetry of the patch's overall structure is essential to acquiring polarization-insensitive and wide-angle characteristic. It is a viable option for sensing applications due to its near-unity absorption and superior sensing capabilities. Paper [20] proposed a wide-angle and polarization-insensitive MMA generating four narrow-band absorptance peaks with electrical dimensions of $0.138\lambda \times 0.138\lambda$ and dual elliptical resonators for microwave electromagnetic interference (EMI) shielding applications. At 3.46 GHz, 6.44 GHz, 7.89 GHz, and 12.44 GHz, respectively, the suggested MMA showed the peak absorptance of 97%, 99.9%, 99.9%, and 99.6%. A unique X-shaped modified SRR quad-band MMA for covert applications in the C, X, and Ku bands is presented in [21]. The MMA has unit cells with dimensions of $0.25\lambda \times 0.254\lambda$ at 7.64 GHz and exhibits absorptance peaks at 7.64 GHz (98.4%), 8.41 GHz (97%), 11.4 GHz (99.2%), and 12.66 GHz (99%), perfect for stealth and shielding against electromagnetic interference (EMI) in defense applications. A quad-band absorber with ultrathin and polarization-insensitive behavior is proposed and produced [22]. It is intended to function in the S, C, and Ku bands with absorption peaks greater than 95%. With overall dimensions of 10 mm × 9.8 mm × 1.00 mm, it finds applications in radio frequency (RF) identification, stealth technology, radar cross-section (RCS) reduction, and EM compatibility. The research [23] demonstrates a quad-band metamaterial absorber with a periodically ordered surface structure on an ultra-thin substrate. Four symmetrically arranged L-shaped structures plus a rectangular patch make up its surface structure. The overall dimensions of the proposed MMA unit cell are 19 mm × 19 mm × 0.8 mm. This research proposes an absorber that could be used for imaging, detecting, filtering, and other communication applications. With a distinctive Y-shaped resonator design, [24] suggested an improved perfect MMA for the microwave band that is ideal for multiple frequencies within the X, Ku, K, and Ka bands. High absorption peaks at four different frequencies are realized. The absorption rates at 10.28 GHz, 16.56 GHz, 22.74 GHz, and 25.96 GHz were 95.7%, 97.3%, 99.8%, and 97.1%, respectively. With unit cell dimensions of 12 mm × 12 mm × 0.8 mm, it finds application in EMI shielding. A small-scale dual-band metamaterial absorber for solid and liquid sensing applications is designed, configured, and investigated in [26]. The unit cell has a star-shaped patch within a square SRR with overall dimensions of $10 \times 10 \times 1.57\,\text{mm}^3$. The absorber showed two absorption peaks at 7.219 GHz in C-band and 3.470 GHz in S-band with absorptance greater than 99%. A dual-band new metamaterial-based 5G absorber [27] is made of symmetric meander lines coupled by a transmission line and operates at 24 GHz and 28 GHz. The overall dimensions of the unit cell are $8 \times 8 \times 1.6\,\text{mm}^3$. The structure with an absorptance of more than 95% is used for absorption in millimeter-wave array antennas.

The designs of multi-band (quad-band) metamaterial absorbers are complicated, have large dimensions, lack an analogous circuit model, and do not have broadband with angular and polarization stability. In light of these constraints, a new quad-band metamaterial absorber design with two broadbands due to merging two frequency bands is suggested. It has a very simple structure, a small-scale design with angular and polarization stable absorptance. It exhibits two absorptance broadbands, one extending from 7.73 GHz–9.54 GHz and the other extending from 10.65 GHz–13.27 GHz. It has applications in wireless communication, stealth technologies, and RCS reduction.

2. DESIGN STRUCTURE OF DBBMDBMMA UNIT CELL

The proposed DBBMDBMMA unit cell is made of a metallic ground plane at the bottom, resonant patches at the top, and a substrate in the middle, as shown in Figure 1. The FR4 substrate is 2 mm thick, having a dielectric constant of 4.3 and a loss tangent of 0.02. Under precisely impedance-matched conditions, patches of the top layer are engineered to optimize absorption and reduce reflection of incident electromagnetic waves at particular frequencies. The metallic ground plane stops incident electromagnetic waves from being transferred as they pass through the substrate. After several internal reflections, reflected EM waves are attenuated inside the substrate. The unit cell measures 18 mm by 18 mm by 2 mm

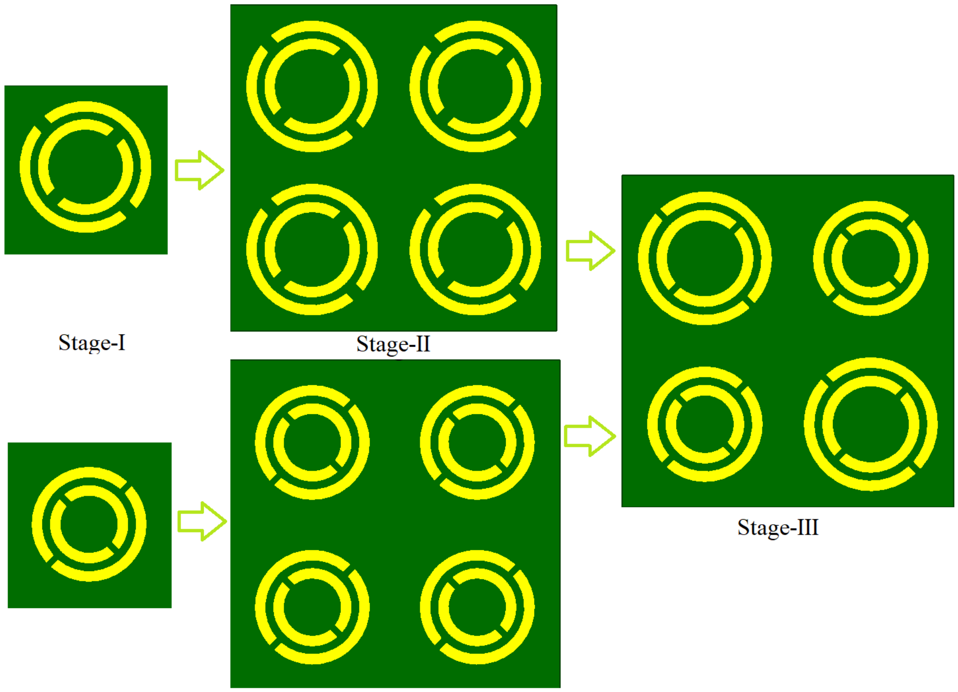

FIGURE 2. Stage-wise optimization of the unit cell.

$(0.5\lambda_o \times 0.5\lambda_o \times 0.05\lambda_o)$, λ_o at 8.5 GHz. The frequency-selective surface (FSS) consists of concentric split-ring resonators ($CSRR^1$ or $CSRR^2$) in each quadrant. $CSRR^2$ are in I and III quadrants, and $CSRR^1$ are in II and IV quadrants. The splits in inner rings and in outer rings are 180° apart and 90° apart with respect to each other. Table 1 shows the unit cell's optimal dimensions.

The "CST Microwave Studio" package was used to run several numerical simulations in order to optimize dimensions. In parametric analysis, one parameter is changed while all other parameters remain unchanged. As seen in Figure 2, the optimization process is carried out in phases. In stage-I, CSRRs are designed in such a way that the inner SRR's dimension of the first pair of SRRs ($CSRR^1$) is the same as the outer SRR's dimension of the second pair of SRRs ($CSRR^2$) with the mindset and simulation trials to have merged bands. In stage-II, $CSRR^1$ are placed in each quadrant, and similarly, $CSRR^2$ are placed in each quadrant. In stage-III, $CSRR^1$ and $CSRR^2$ are mixed in such a way that quadrants I and III have $CSRR^2$ and quadrants II and IV have $CSRR^1$.

3. EQUIVALENT CIRCUIT MODEL OF DBBMDBMMA UNIT CELL

Each metallic strip can be represented as an inductor and a capacitor used to mimic the space between two metallic conductors in the MMA's equivalent circuit, which is created using transmission line theory. The FR4 substrate acts as a gap between top-layer CSRRs and the ground plane; therefore, the outer and inner resonators of $CSRR^1$, together with the ground plane, are modeled as L_1C_1 and L_2C_2, respectively. Similarly, outer and inner resonators of $CSRR^2$ together with ground plane are modeled as L_3C_3 and L_4C_4, respectively, as shown in Figures 3(a) and 4(a). Both capacitive and inductive effects may be seen in the mutual connection between two concentric split square ring resonators. There are also parasitic capacitances between the MMA and ports. Since the substrate aids in signal absorption, it can be compared to the energy-consuming resistor in an electrical circuit. After taking all these factors into consideration, the model of an analogous circuit is shown in Figures 3(b) and 4(b).

TABLE 1. Optimal unit cell dimensions.

Parameter	Dimension (mm)	Parameter	Dimension (mm)
x_1	18	y_1	18
r_1	3.6	r_2	3.1
r_3	2.6	r_4	2.1
g_1	0.5	g_2	0.5

For the DBBMDBMMA unit cell's optimal dimensions listed in Table 1, the resonance frequency (fr) for a particular resonator structure for maximum absorptance is calculated using Eq. (7) [25], where C_{SRR} and L_{SRR} are evaluated using Eqs. (1) and Eq. (6) [25].

$$C_{SRR} = \frac{N-1}{2}\{2*L-(2*N-1)*(t+s)\} * \left\{\varepsilon_0\left(\frac{1+\varepsilon_r}{2}\right)\left(\sqrt{1-k^2}\right)\right\} \quad (1)$$

$$k = \frac{s}{(s+2t)} \quad (2)$$

$$L_{avg} = 4*\{L-(N-1)(t+s)\} \quad (3)$$

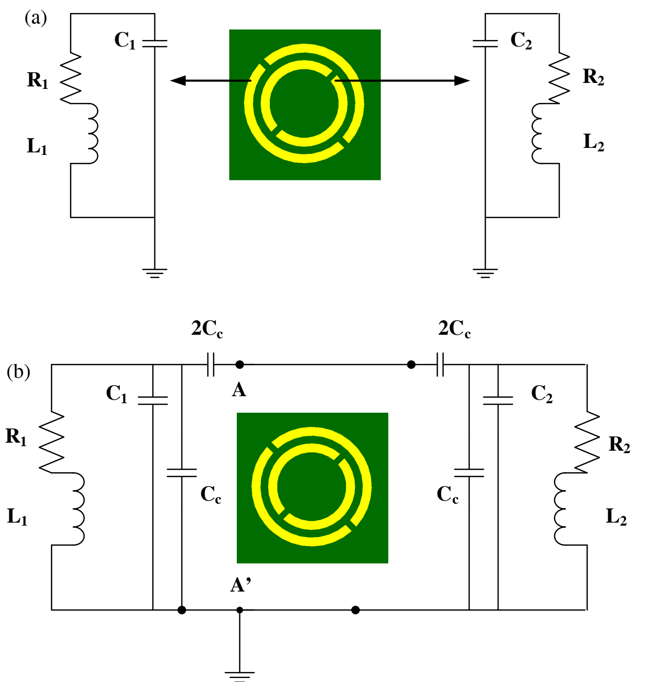

FIGURE 3. (a) Individual circuit model of CSRR[1] and (b) equivalent circuit model of CSRR[1]

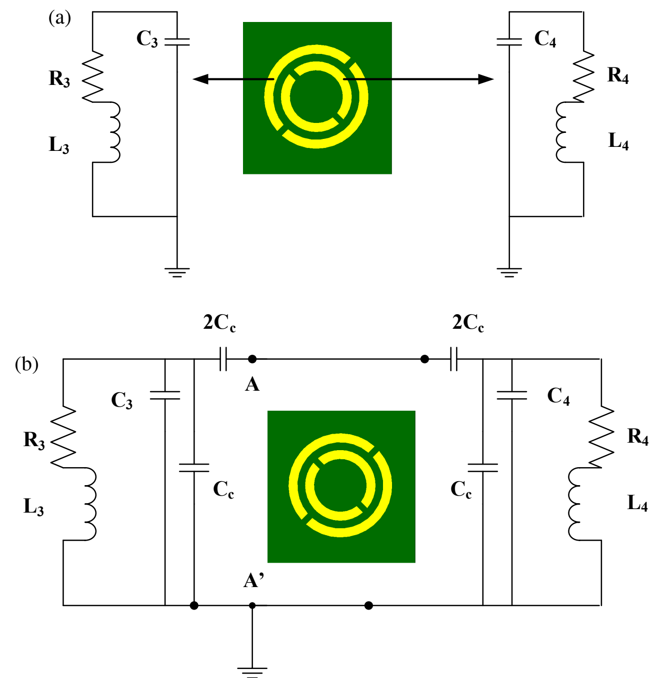

FIGURE 4. (a) Individual circuit model of CSRR[2] and (b) equivalent circuit model of CSRR[2].

$$L_{SRR} = \left\{\frac{\mu_0}{2}\frac{L_{avg}}{4}\right\}(4.86) * \left\{\ln\left(\frac{0.98}{\rho}\right) + 1.84\rho\right\} \quad (4)$$

$$\rho = \frac{(N-1)(s+t)}{L-(N-1)(s+t)} \quad (5)$$

$$L_{SRR} = \frac{\mu_0}{2}(4.86)\left[L-(N-1)(t+s)\right] * \left\{\ln\left(\frac{0.98}{\rho}\right) + 1.84\rho\right\} \quad (6)$$

$$f_x = \frac{1}{2\pi\sqrt{(L_{SRR})(C_{SRR})}} \quad (7)$$

In the given Eqs. (1)–(7), N is the number of SRR rings; L is the length of outer most ring; s is the distance between rings; t is the width of the strip; ε_r is the substrate's relative permittivity; ε_o is the free space's permittivity; and μ_o is the free space's permeability.

4. DBBMDBMMA UNIT CELL SIMULATION

In the simulation configuration shown in Figure 5, unit cells are placed along the X and Y axes in a grid-like fashion, having an open barrier that allows waves to travel along the Z axis. The EM computational solver "CST microwave studio suite" is used to model the suggested DBBMDBMMA unit cell. This solver evaluates EM-field equations by numerical analysis using the finite element method (FEM). Using Maxwell's equations, the EM solver divides the test device into tetrahedral or hexahedral meshes and calculates how these meshes interact with electromagnetic waves (the proposed design has 91,714 tetrahedral meshes). By accounting for resonances, reflections, and refractions, based on the chosen excitation and applied boundary conditions, CST calculates fields around the material. E- and H-field boundaries are placed along the X and Y axes, respectively, whereas waveguide ports are oriented along the Z-axis in the simulation configuration. The EM wave from port 1 excites the DBBMDBMMA structure, and under normalized impedance-matched conditions with near-zero reflection, causes the proposed structure to resonate at 8.51 GHz, 8.95 GHz, 11.24 GHz, and 12.86 GHz. After the received EM wave passes through the substrate layer, the ground copper layer blocks its transmission. There is no transmission because its thickness is greater than the skin depth. Thus, the required frequency signal is trapped inside the substrate, undergoes many internal reflections, and is eventually absorbed in the middle (substrate) layer. Eq. (8) [7] is used to compute the absorptance $A(f)$, where S_{11} is the "reflectance", and S_{21} is the "transmittance". Since the ground plane prevents EM waves from passing through the absorber, the "transmittance" is zero, and the absorptance depends only on the "reflectance", which is determined by Eq. (9) [7].

$$A(f) = 1 - S_{11}^2 - S_{21}^2 \quad (8)$$

$$A(f) = 1 - S_{11}^2 \quad (9)$$

Under normalized impedance conditions, the unit cell's dimensions are tailored to match the surface impedance with the free space impedance; therefore, simulated reflection coefficients of -24.58 dB at 8.51 GHz, -27.66 dB at 8.95 GHz, -12.58 dB at 11.24, and -17.81 dB at 12.86 GHz for normal incidence of EM waves are obtained as depicted in Figure 6. The absorptance of the obtained reflectance is estimated using Eq. (9), depicted in Figure 7. The simulated absorptances

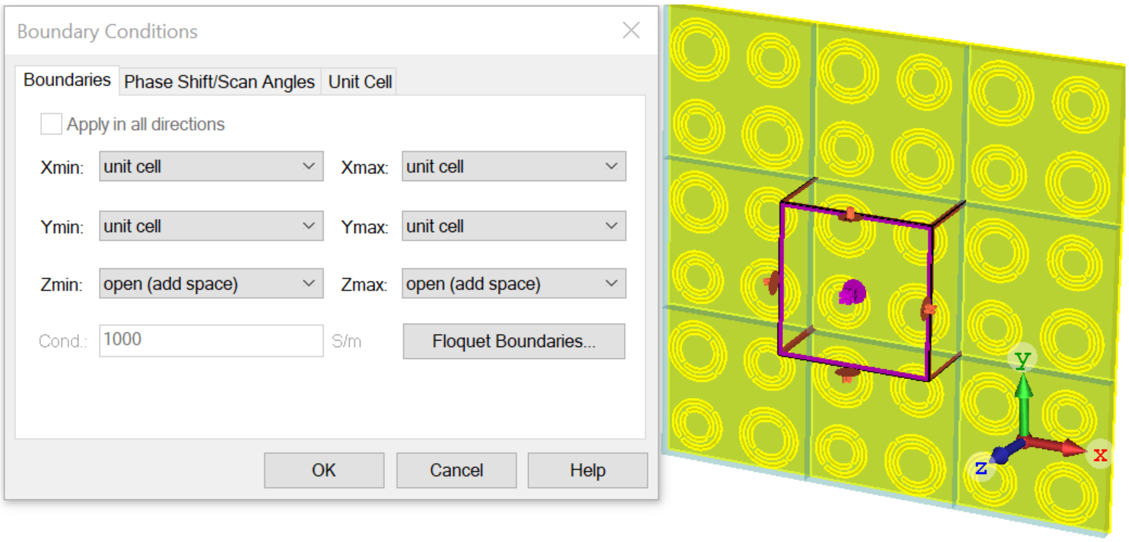

FIGURE 5. Boundary conditions applied to the DBBMDBMMA unit cell.

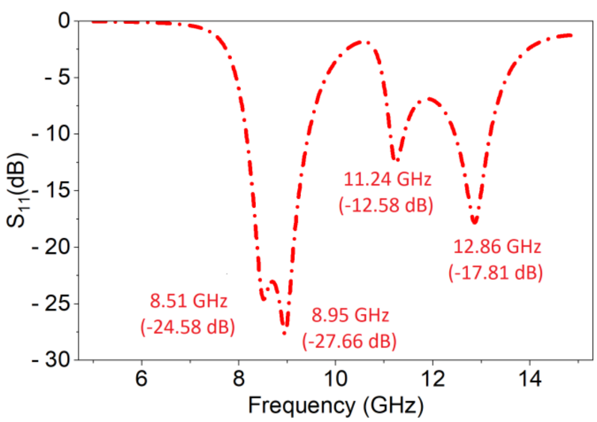

FIGURE 6. Reflectance $S_{11}(f)$ of the DBBMDBMMA structure.

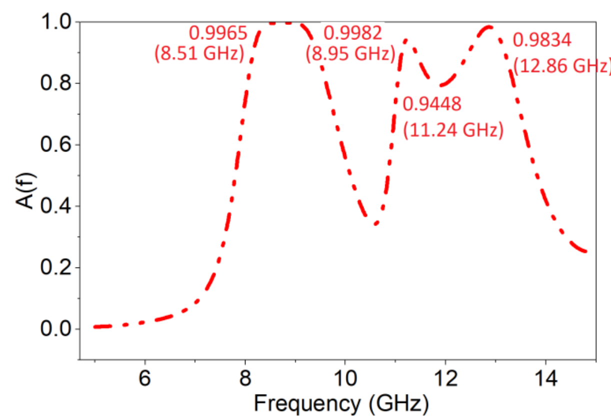

FIGURE 7. Linear absorptance $A(f)$ and reflectance $S_{11}(f)$.

are 99.65% (at 8.51 GHz), 99.82% (at 8.95 GHz), 94.48% (at 11.24 GHz), and 98.34% (at 12.86 GHz) as depicted in Table 2. Due to design novelty, absorptance peaks at 8.51 GHz and 8.95 GHz merged to generate the first absorptance broadband with average peak to peak absorptance of 99.62%, and absorptance peaks at 11.24 GHz and 12.86 GHz merged to generate the second absorptance broadband with average peak to peak absorptance of 87.31%. The two broadbands due to merged dual bands cover X- and Ku-bands, respectively.

TABLE 2. Simulated results of the DBBMDBMMA unit cell.

Frequency (GHz)	$S_{11}(f)$ (dB)	$A(f)$ (%)
8.51	−24.58	99.65
8.95	−27.66	99.82
11.24	−12.58	94.48
12.86	−17.81	98.34
Broad-band I: 7.95 GHz–9.79 GHz		
Broad-band II: 10.97 GHz–13.52 GHz		

The structure's surface current density is calculated to fully comprehend the absorption mechanism at 8.51 GHz, 8.95 GHz, 11.24, and 12.86 GHz. Surface currents at different resonant frequencies depend on MMA resonant properties, which are produced when time-varying electromagnetic waves typically strike the proposed DBBMDBMMA structure parallel to the axis of resonating structures, as shown in Figure 8. The direction of the surface current is indicated by arrows, and its intensity is indicated by different colors. The incident electromagnetic field is either reinforced or counteracted by a magnetic field created by induced currents. Each split ring is a resonator, resonating at a specific frequency where absorption occurs. Strong coupling between resonator structures (split rings in $CSRR^1$ and $CSRR^2$) is produced by the unit cell's periodic array, which increases EM wave absorption, and unique characteristics of negative permeability and permittivity are produced by the composite MMA structure. In Figure 8, surface current patterns clearly indicate that each split-ring resonator is responsible for absorption at some specific frequency. As indicated by simulated results, at 8.51 GHz frequency, the surface current is distributed on the outer split ring of $CSRR^1$, and at

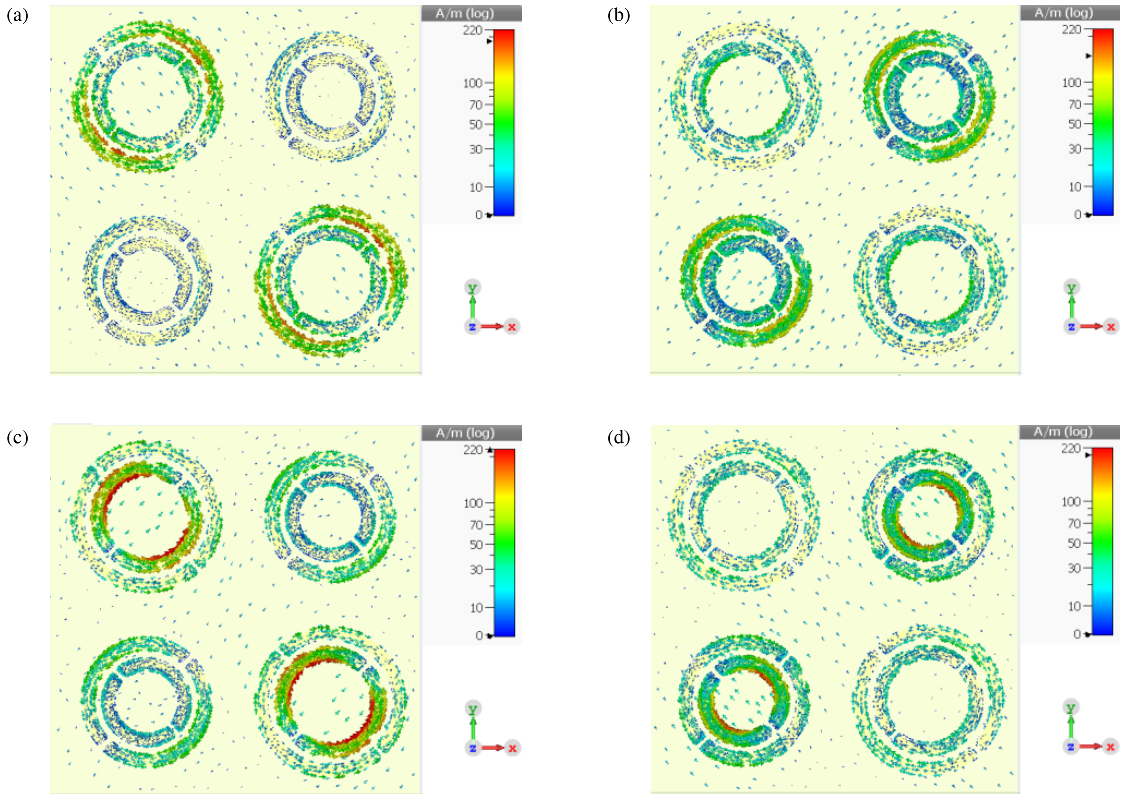

FIGURE 8. Surface current distribution at (a) 8.51 GHz, (b) 8.95 GHz, (c) 11.24 GHz, and (d) 12.86 GHz.

8.95 GHz frequency; the surface current is distributed on the outer split ring of CSRR^2; at 11.24 GHz frequency, the surface current is distributed on the inner split ring of CSRR^2; at 12.86 GHz frequency, the surface current is distributed on the inner split ring of CSRR^1. It may be concluded that the outer split rings of CSRR^1 and CSRR^2 are responsible for absorptance at 8.51 GHz and 8.95 GHz, respectively, and inner split rings of CSRR^1 and CSRR^2 are responsible for absorptance at 11.24 GHz and 12.86 GHz, respectively. Due to design novelty, the dual absorptance bands generated by outer split rings of CSRR^1 and CSRR^2 which are merged to generate the first broadband extending from 7.95 GHz to 9.79 GHz and the dual absorptance bands generated by inner split rings of CSRR^1 and CSRR^2 are merged to generate the second broadband extending from 10.97 GHz to 13.52 GHz as depicted in Table 2.

The same absorption dominance is recorded by the H-field pattern where for the first absorptance band, the H-field is distributed on the outer split ring of CSRR^1; for the second absorptance band, the H-field is distributed on outer split ring of CSRR^2; for third absorptance band, the H-field is distributed onthe inner split ring of CSRR^1; for the fourth absorptance band, the H-field is distributed on the inner split ring of CSRR^2, as depicted in Figures 9(a)–(d).

5. METAMATERIAL BEHAVIOUR OF DBBMDBMMA STRUCTURE

Two requirements must be fulfilled for an absorber to show metamaterial behavior. The incident EM wave must be accurately impedance-matched with that of the MMA's top layer in order to be completely transmitted into the MMA without reflections. Additionally, for the absorbed EM wave to be highly dissipated within the MMA, a high imaginary value of the permeability and permittivity is required [7]. As $\mathrm{Re}[Z_{\mathit{eff}}(f)]$ approaches 1 and $\mathrm{Im}[Z_{\mathit{eff}}(f)]$ approaches 0, Figure 10 verifies impedance matching at maximal absorptance peaks. Eq. (10) is used to estimate normalized impedance-matched values. Effective impedance, $Z_{\mathit{eff}}(f)$, and effective permeability, $\mu_{\mathit{eff}}(f)$, are calculated using S_{11} and S_{21} parameters to examine the metamaterial behavior of the suggested MMA. Effective permeability, which is determined by Eq. (11) [7], is influenced by the MMA structural design and contributes to the medium's efficacy. Effective permeability has real and imaginary values. Real values show Lorentzian transitions, negative to positive or positive to negative, which aids metamaterial behavior, as shown in Figure 11. High imaginary values account for the dissipation of EM waves inside the substrate after multiple reflections from the ground plane.

$$Z_{\mathit{eff}}(f) = \sqrt{\frac{[1+S_{11}(f)]^2 - S_{21}^2(f)}{[1-S_{11}(f)]^2 - S_{21}^2(f)}} \tag{10}$$

$$\mu_{\mathit{eff}}(f) = \frac{2}{jk_o d}\left(\frac{1+S_{11}-S_{21}}{1-S_{11}+S_{21}}\right) \tag{11}$$

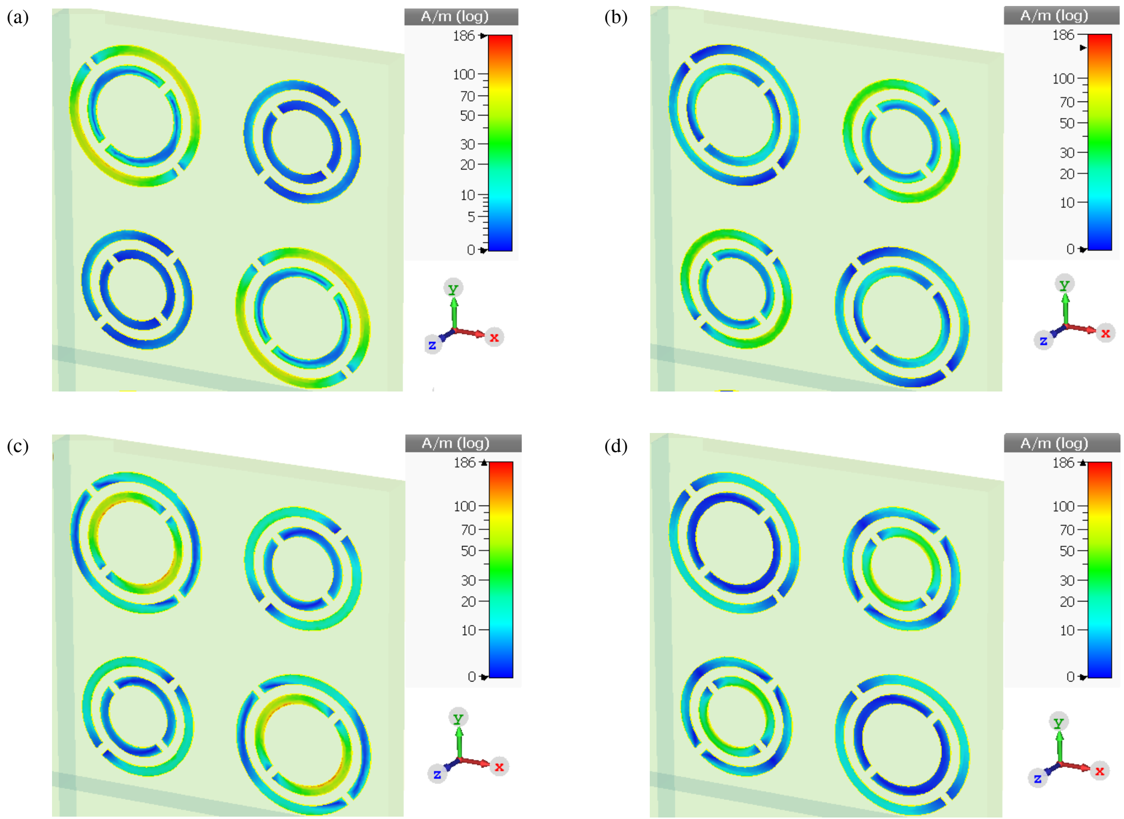

FIGURE 9. H-field distribution at (a) 8.51 GHz, (b) 8.95 GHz, (c) 11.24 GHz, and (d) 12.86 GHz.

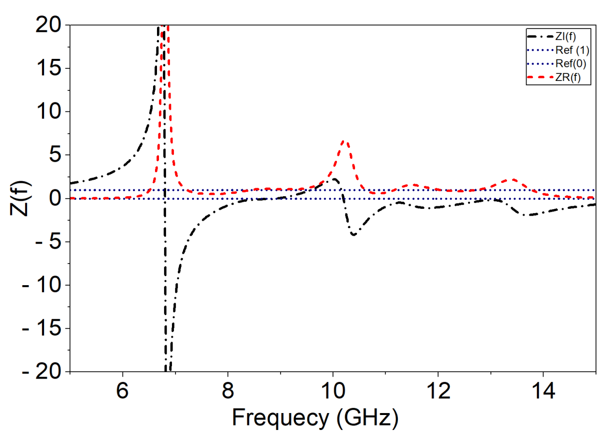

FIGURE 10. Real and imaginary impedance values of the DBBMDB-MMA structure.

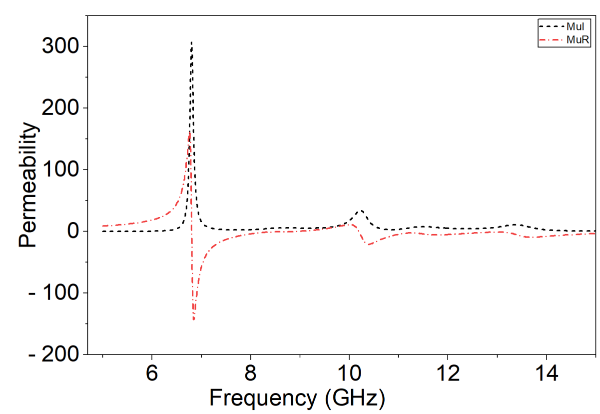

FIGURE 11. Effective values of (a) permeability μ_{eff} (f) of DBBMDB-MMA structure.

6. EXPERIMENTAL SETUP AND MEASURED RESULTS

Figure 12 depicts the experiment. The Agilent Technologies N5230A, 10 MHz–50 GHz Vector Network Analyzer (VNA) and a horn antenna covering the whole range were used for the test. The VNA was adjusted for accuracy across the frequency range of 1 GHz to 18 GHz before conducting measurements. The measurement takes place within an anechoic chamber, surrounded by foam-based conventional absorbers that eradicate unwanted reflected signals. The reflectance measurement is done in two steps. In the first step, the reflectance $S_{11}(f)$ from a same-size copper sheet was measured to account free-space losses. Subsequently, in the second step, the prototype DBBMDBMMA structure was aligned at an identical position to measure its reflectance $S_{11}(f)$ with the help of a horn antenna and a connected VNA. The horn antenna transmits EM waves and receives reflected EM waves, and the reflectance was measured by the VNA connected to the horn antenna. The corrected calibrated reflectance $S_{11}(f)$ is calculated with the difference between two measured values, and the absorptance is estimated using Eq. (9). The same measurement process is implemented to record the reflectance for variation in angle of incidence (θ) and angle of polarization (φ).

FIGURE 12. Experiment setup (anechoic chamber).

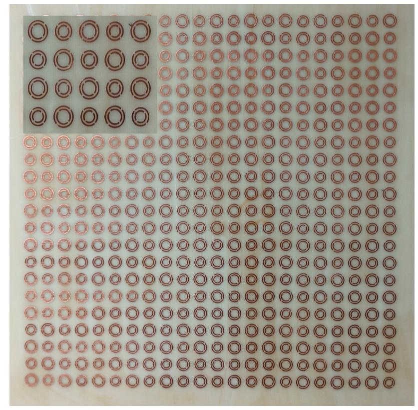

FIGURE 13. Fabricated DBBMDBMMA structure.

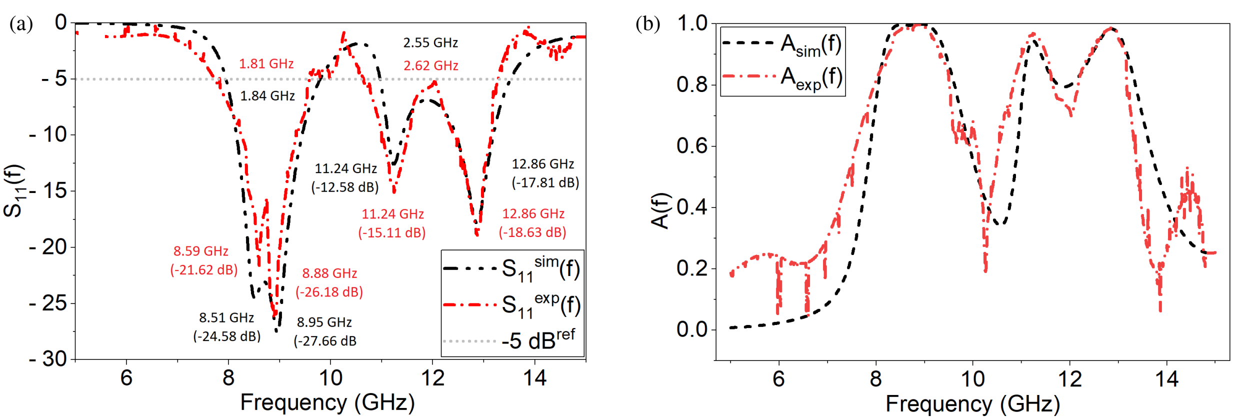

FIGURE 14. Comparison of (a) simulated and measured reflectance and (b) simulated and estimated absorptance.

TABLE 3. Simulated versus measured results of the DBBMDBMMA structure.

Simulated Results			Experimental Results		
Resonance Frequency (GHz)	**S_{11} (dB)**	**A (f)**	**Resonance Frequency (GHz)**	**S_{11} (dB)**	**A (f)**
8.51	−24.58	99.65	8.59	−21.62	99.31
8.95	−27.66	99.82	8.88	−26.18	99.75
11.24	−12.58	94.48	11.24	−15.11	96.91
12.86	−17.81	98.34	12.86	−18.63	98.62
Broad-band I Bandwidth (−5 dB): 1.84 GHz			Broad-band I Bandwidth (−5 dB): 1.81 GHz		
Broad-band II Bandwidth (−5 dB): 2.55 GHz			Broad-band II Bandwidth (−5 dB): 2.62 GHz		

The prototype of the proposed DBBMDBMMA structure is fabricated on a double-sided FR4 substrate that consists of 121 unit cells with 11 rows and 11 columns, with overall dimensions of 198 mm × 198 mm × 2 mm, as shown in Figure 13. The suggested DBBMDBMMA structure was created using the processes of photolithography and wet etching. The reflection coefficient $S_{11}(f)$ in free space has been measured using the far-field approach. When the two-step measuring procedure mentioned above is used for normal EM wave incidence, the reflectance is found to be −21.62 dB (at 8.59 GHz), −26.18 dB (at 8.88 GHz), −15.11 dB (at 11.24 GHz), and −18.63 dB (at 12.86 GHz) in contrast to simulated reflectance of −24.58 dB (at 8.51 GHz), −27.66 dB (at 8.95 GHz), −12.58 dB (at 11.24 GHz), and −17.81 dB (at 12.86 GHz), as shown in Figure 14(a) and depicted in Table 3. The absorptance is estimated using Eq. (9), and the values are depicted in Figure 14(b). The third and fourth simulated and measured resonance frequency values are the same, whereas the first and second simulated and measured resonance frequency values have slight variations. This is probably due to fabrication errors. The proposed design is fabricated by the wet etching method using the photolithography process.

TABLE 4. Comparative study and analysis of the DBBMDBMMA structure with reported MMA designs.

Ref.	Unit cell design	Design difficulty	Dimensions (λ at Lowest Frequency)	Freq. bands Freq.(GHz) S_{11} (dB) or Abs.(%)	Ang. stability	Pol. stability	Broad-band (GHz)	Eq. ckt	Applications
[18] 2024	Four-square SRRs with an inner star	moderate	0.156λ x 0.156λ x 0.0156λ	4.68 (86.97) 6.43 (99.74) 8.08 (99.95) 10.97 (98.43)	No	No	No	Yes	Sensing
[19] 2022	An inner Jerusalem, two square SRRs, and four microstrip lines	complex	0.42λ x 0.42λ x 0.067λ	12.62 (97) 14.12 (99.51) 17.53 (99) 19.91 (99.5)	Yes	Yes	No	Yes	Sensing
[20] 2023	Dual elliptical resonators	complex	0.138λ x 0.138λ x 0.0185λ	3.46 (97) 6.44 (99.9) 7.89 (99.9) 12.44 (99.6)	Yes	Yes	No	Yes	EMI shielding
[21] 2025	X-shaped modified SRR	complex	0.254λ x 0.254λ x 0.0407λ	7.64 (98.4) 8.41 (97) 11.4 (99.2) 12.66 (99)	Yes	Yes	No	Yes	EMI shielding and stealth
[22] 2023	Eight armed asterick shaped enclosed in a square ring with trimmed edges	complex	0.103λ x 0.103λ x 0.0103λ	3.1 (99.37) 5.42 (99.04) 16.65 (98.61) 17.56 (95.12) 20.29 (95.57)	Yes	Yes	No	No	Stealth technology, RCS reduction, and EM compatibility
[23] 2023	Rectangular patch with four L-shaped structures	moderate	0.297λ x 0.297λ x 0.0125λ	4.70 (90.89) 10.19 (90.18) 11.96 (94.80) 14.15 (90.02)	Yes	Yes	No	No	Imaging, detecting, and filtering
[24] 2026	Four Y-shaped resonators	moderate	0.41λ x 0.41λ x 0.0274λ	10.28 (95.7) 16.56 (97.3) 22.74 (99.8) 25.96 (97.1)	Yes	Yes	No	No	EMI shielding, radar systems
[26] 2024	Star shaped patch within square SRR	moderate	0.115λ x 0.115λ x 0.018λ	3.470 (99.8) 7.219(99.5)	No	No	No	No	Sensing
[27] 2022	Two pairs of meander lines with an I-shape	Medium	0.64λ x 0.64λ x0.128λ	24 (98) 28 (95)	Yes	Yes	No	Yes	5G communication
Proposed	Concentric SRRs in four quadrants	Simple	0.5λ x 0.5λ x 0.05λ	8.59 (99.31) 8.88 (99.75) 11.24 (96.91) 12.86 (98.62)	Yes	Yes	Yes 02 1.81 2.62	Yes	Stealth technology, RCS reduction, 5G communication

There may be chances of over etching the copper from the top frequency-selective layer.

However, an incident wave will not always be incident normally on the MMA in real-world applications. When EM waves arrive at any angle, a perfect MMA should have a stable and similar response. Therefore, incidence angle (θ) and polarization angle (φ) variations are used to measure angular stability. The suggested DBBMDBMMA structure response is depicted in Figure 16(a) with polarization angle variations ($\varphi = 0^\circ$, $\varphi = 90^\circ$, $\varphi = 180^\circ$). The response is stable and comparable, and the results show that the suggested DBBMDBMMA structure is insensitive to polarization. As shown in Figure 15(a), the MMA response is also examined with variations in incident angle ($\theta = 10^\circ, \theta = 20^\circ, \theta = 30^\circ$, and $\theta = 40^\circ$). The findings demonstrate that the response of the suggested DBBMDBMMA structure is impacted beyond 40 degrees as the incident angle increases, with decreased surface availability to incident EM waves. The findings indicate that the response to the change in incident angle is also insensitive.

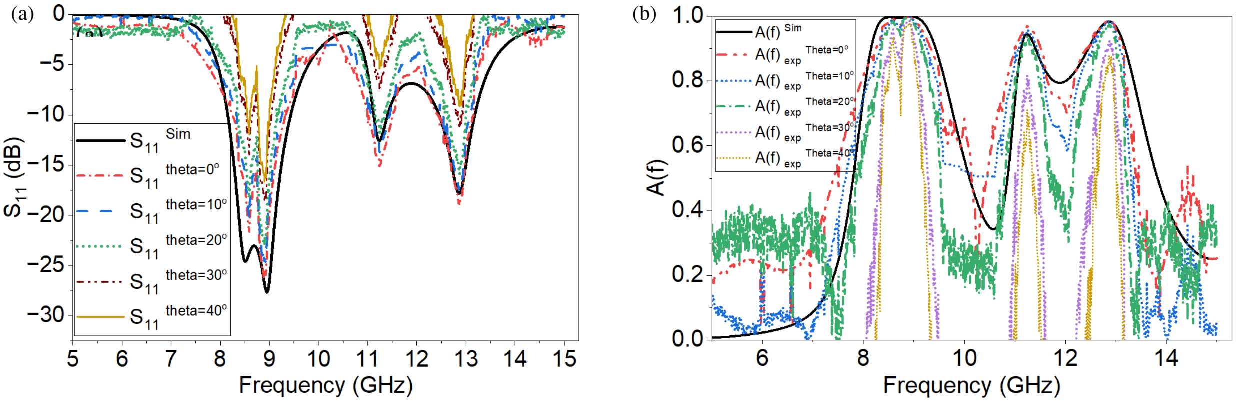

FIGURE 15. (a) Reflectance measurement and (b) absorptance estimation with variation in incidence angle (θ).

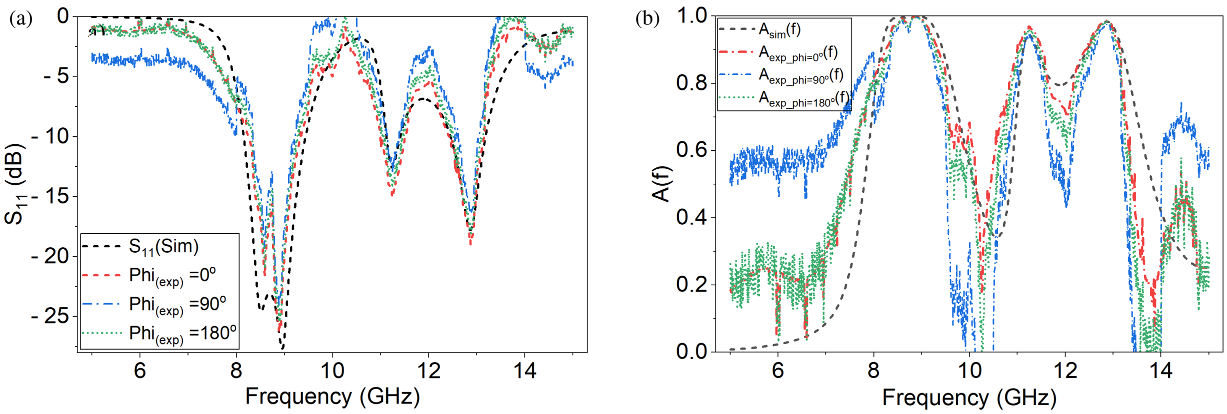

FIGURE 16. (a) Reflectance measurement and (b) absorptance estimation with variation in polarization angle (ϕ).

7. CONCLUSION

A novel MMA design that consists of CSRR^1 in II and IV quadrants and CSRR^2 in I and III quadrants is simulated on "CST microwave suite", fabricated using "photolithography and wet etching process", and tested in an "anechoic chamber". High absorptance in terms of dual bands with merged double bands is achieved by artificially engineering and optimizing dimensions of CSRR^1 and CSRR^2 in four quadrants. Unit cell dimensions of the proposed DBBMDBMMA are 18 mm $\times$ 18 mm $\times$ 2 mm. The fabricated MMA has overall dimensions of 198 mm $\times$ 198 mm $\times$ 2 mm with 121 unit cells arranged in 11 rows and 11 columns. The proposed DBBMDBMMA structure exhibited absorptance at 8.59 GHz, 8.88 GHz, 11.24 GHz, and 12.86 GHz with reflectance (absorptance) of -21.62 dB (99.31%), -26.18 dB (99.75%), -15.11 dB (96.91%), and -18.63 dB (98.62%), respectively. Absorption behavior and contribution of specific resonating patches to absorptance bands are investigated by analyzing the surface current distribution. The analysis revealed that the outer SRR of CSRR^1 contributes to the first absorptance band; the outer SRR of CSRR^2 contributes to the second absorptance band; inner SRRs of CSRR^1 and CSRR^2 contribute to the third and fourth absorptance bands. The merged effect of the first and second absorptance bands results in the first dual-band response with a broadband of 1.81 GHz, and the merged effect of the third and fourth absorptance bands results in the second dual-band response with a broadband of 2.62 GHz. To investigate the metamaterial behavior, effective values of normalized matched impedance and effective permeabilty are examined. It is experimentally verified that the response of the suggested DBBMDBMMA structure is stable at normal EM wave incidence and with changes in the incidence angle (θ) and polarization angle (φ). In terms of "unit cell design", "design difficulties", "optimized unit cell dimensions", "absorptance bands", "dual-band absorptance", "angular stability", "polarization stability", "broadband", and "analogous circuit model", the suggested DBBMDBMMA structure is compared with previously published (2022–2026) MMA designs. The suggested DBBMDBMMA structure clearly outperforms reported designs in design simplicity, high and stable response against θ and φ variations, and two absorptance broadbands located in X- and Ku-bands, which find application in stealth technology and RCS reduction, as shown in the comparison analysis of Table 4.

REFERENCES

[1] Veselago, V. G., "The electrodynamics of substances with simultaneously negative values of ε and μ," *Soviet Physics Uspekhi*, Vol. 10, No. 4, 509–514, 1968.

[2] Cui, H., H. Gao, L. Lu, and G. Hu, "Ultra-thin broadband metamaterial absorber with a simple cylindrical structure," *Plasmonics*, Vol. 20, No. 7, 5059–5068, 2025.

[3] Pendry, J. B., D. Schurig, and D. R. Smith, "Controlling electromagnetic fields," *Science*, Vol. 312, No. 5781, 1780–1782, 2006.

[4] Alsulami, Q. A., S. Wageh, A. A. Al-Ghamdi, R. M. H. Bilal, and M. A. Saeed, "A tunable and wearable dual-band metamaterial absorber based on polyethylene terephthalate (PET) substrate for sensing applications," *Polymers*, Vol. 14, No. 21, 4503, 2022.

[5] Gai, Y., S. Zhou, and G. Lan, "Ultra-broadband perfect metamaterial absorber for solar energy harvesting," *Plasmonics*, Vol. 20, No. 7, 5145–5153, 2025.

[6] Rakhshani, M. R., F. Kazemi, and M. Rashki, "Metamaterial absorber using cascaded ring resonators and optimization through machine learning for sensing applications," *Scientific Reports*, Vol. 15, No. 1, 39977, 2025.

[7] Agrawal, A. and M. Misra, "Angle of incidence and polarization insensitive ultra-thin ultra wide-band metamaterial absorber based on novel non-linearity in unit cell design," *Journal of Microwaves, Optoelectronics and Electromagnetic Applications*, Vol. 20, No. 3, 556–569, 2021.

[8] Rahman, A. A. M., M. T. Islam, M. Moniruzzaman, H. Alsaif, A. A. Maash, M. M. Hasan, and M. S. Soliman, "Resonator-based near perfect metamaterial absorber with high EMI shielding for Wi-Fi and 5G applications," *International Journal of Optomechatronics*, Vol. 18, No. 1, 2375497, 2024.

[9] Geng, J., X.-H. Deng, Z. Xiong, J. Gao, and B. Song, "Innovative design to achieve a multi-band electromagnetic wave stealth," *Optics Letters*, Vol. 49, No. 18, 5328–5331, 2024.

[10] Geng, J., X.-H. Deng, Z. Xiong, J. Gao, B. Song, and J. Yuan, "Ultra-wideband terahertz absorber with switchable multiple modes based on graphene and vanadium dioxide metamaterials," *Chinese Journal of Physics*, Vol. 92, 1312–1324, 2024.

[11] Geng, J., X.-H. Deng, Z. Xiong, J. Gao, B. Song, and Y. Lou, "A metasurface capable of simultaneous stealth across multiple electromagnetic wave bands and its design concept," *Composites Communications*, Vol. 55, 102328, 2025.

[12] Murali Naik, K. H., A. K. Singh, and D. R. Krishna, "Ultrathin wideband low profile circuit analog metamaterial absorber," *Microwave and Optical Technology Letters*, Vol. 66, No. 7, e34247, 2024.

[13] Shruti, , S. Pahadsingh, and B. Appasani, "Metamaterial-based terahertz absorbers for refractive index sensing: Types, mechanism, and applications," *Plasmonics*, Vol. 20, No. 7, 5557–5571, 2025.

[14] Landy, N. I., S. Sajuyigbe, J. J. Mock, D. R. Smith, and W. J. Padilla, "Perfect metamaterial absorber," *Physical Review Letters*, Vol. 100, No. 20, 207402, 2008.

[15] Özer, Z., V. Akdoğan, L. Wang, and M. Karaaslan, "Graphene-based tunable metamaterial absorber for terahertz sensing applications," *Plasmonics*, Vol. 19, No. 6, 3381–3391, 2024.

[16] Zhang, D., Y. Chen, and Q. Zhou, "Multilayer broadband metamaterial for microwave absorption based on resistive frequency selective surfaces," *Results in Physics*, Vol. 73, 108261, 2025.

[17] Cao, Z., X. Zeng, and G. Lan, "Ultra-broadband metamaterial absorber for near-infrared and mid-infrared applications optimized via deep learning," *Applied Optics*, Vol. 64, No. 25, 7527–7533, 2025.

[18] Sakib, S., A. Hoque, M. T. Islam, A. M. Alenezi, M. S. Soliman, and H. Alsaif, "Design and analysis of quad-band metamaterial absorber for permittivity sensing with phase evolved equivalent circuit analysis," *Ain Shams Engineering Journal*, Vol. 15, No. 12, 103153, 2024.

[19] Hakim, M. L., T. Alam, M. T. Islam, M. H. Baharuddin, A. Alzamil, and M. S. Islam, "Quad-band polarization-insensitive square split-ring resonator (SSRR) with an inner Jerusalem cross metamaterial absorber for Ku-and K-Band sensing applications," *Sensors*, Vol. 22, No. 12, 4489, 2022.

[20] Hossain, M. B., M. R. I. Faruque, and M. T. Islam, "Double elliptical resonator based quadruple band metamaterial absorber for EMI shielding applications in microwave regime," *Alexandria Engineering Journal*, Vol. 69, 193–206, 2023.

[21] Hussain, A., J. Dong, Y. I. Abdulkarim, R. Shi, B. Colak, M. Karaaslan, S. S. Hussain, and W. Ali, "Quad-band metamaterial absorber with high shielding effectiveness using bold X-shaped ring resonator," *Journal of Electronic Materials*, Vol. 55, No. 2, 2240–2257, 2026.

[22] Singh, R. K., A. Gupta, A. Yadav, N. Gupta, and U. Tyagi, "An ultrathin polarization free asterick-shaped metamaterial absorber with quad-band characteristics," *International Journal of Antennas and Propagation*, Vol. 2023, No. 1, 5664588, 2023.

[23] Jin, S., H. Zu, W. Qian, K. Luo, Y. Xiao, R. Song, and B. Xiong, "A quad-band and polarization-insensitive metamaterial absorber with a low profile based on graphene-assembled film," *Materials*, Vol. 16, No. 11, 4178, 2023.

[24] Al-Badri, K. S. L., "High-efficiency multi-band metamaterial absorber for X to Ka band applications," *Kuwait Journal of Science*, Vol. 53, No. 1, 100514, 2026.

[25] Mishra, P., B. P. Singh, and V. V. Agrawal, "Deciphering split ring resonators: Understanding theoretical validation and simulation implications," *Engineering Research Express*, Vol. 6, No. 3, 035319, 2024.

[26] Khalil, M. A., W. H. Yong, M. S. Islam, L. Y. Chiong, A. Hoque, N. Ullah, H. H. Goh, T. A. Kurniawan, M. S. Soliman, and M. T. Islam, "Design of dual peak star shaped metamaterial absorber for S and C band sensing applications," *Scientific Reports*, Vol. 14, No. 1, 26609, 2024.

[27] Naqvi, S. A., M. A. Baqir, G. Gourley, A. Iftikhar, M. S. Khan, and D. E. Anagnostou, "A novel meander line metamaterial absorber operating at 24 GHz and 28 GHz for the 5G applications," *Sensors*, Vol. 22, No. 10, 3764, 2022.